

Pixel-wise Gradient Uncertainty for Convolutional Neural Networks applied to Out-of-Distribution Segmentation

Kira Maag*¹

Tobias Riedlinger*²

¹Ruhr University Bochum, Germany, kira.maag@rub.de

²University of Wuppertal, Germany, riedlinger@math.uni-wuppertal.de

Abstract

In recent years, deep neural networks have defined the state-of-the-art in semantic segmentation where their predictions are constrained to a predefined set of semantic classes. They are to be deployed in applications such as automated driving, although their categorically confined expressive power runs contrary to such open world scenarios. Thus, the detection and segmentation of objects from outside their predefined semantic space, i.e., out-of-distribution (OoD) objects, is of highest interest. Since uncertainty estimation methods like softmax entropy or Bayesian models are sensitive to erroneous predictions, these methods are a natural baseline for OoD detection. Here, we present a method for obtaining uncertainty scores from pixel-wise loss gradients which can be computed efficiently during inference. Our approach is simple to implement for a large class of models, does not require any additional training or auxiliary data and can be readily used on pre-trained segmentation models. Our experiments show the ability of our method to identify wrong pixel classifications and to estimate prediction quality. In particular, we observe superior performance in terms of OoD segmentation to comparable baselines on the SegmentMeIfYouCan benchmark, clearly outperforming methods which are similarly flexible to implement.

1 INTRODUCTION

Semantic segmentation decomposes the pixels of an input image into segments which are assigned to a fixed and predefined set of semantic classes. In recent years, deep neural networks (DNNs) have performed excellently in this task [Chen et al., 2018, Wang et al., 2021], providing com-

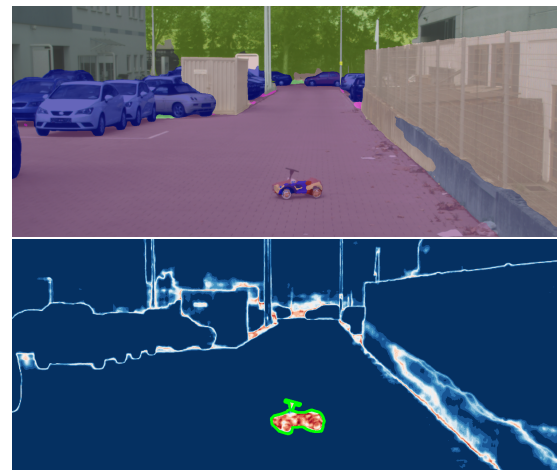


Figure 1: *Top*: Semantic segmentation by a state-of-the-art deep neural network. *Bottom*: Gradient uncertainty heatmap obtained by our method.

prehensive and precise information about the given scene. However, in safety relevant applications like automated driving where semantic segmentation is used in open world scenarios, DNNs often fail to function properly on unseen objects for which the network has not been trained, see for example the bobby car in Figure 1 (top). These objects from outside the network’s semantic space are called out-of-distribution (OoD) objects. It is of highest interest that the DNN identifies these objects and abstains from deciding on the semantic class for those pixels covered by the OoD object. Another case are OoD objects which might belong to a known class, however, appearing differently to substantial significance from other objects of the same class seen during training. Consequently, the respective predictions are prone to error. For these objects, as for classical OoD objects, marking them as OoD is preferable to the likely case of misclassification which may happen with high confidence. Furthermore, this additional classification task should not substantially degrade the semantic segmentation performance itself outside the OoD region. The computer

* equal contribution

vision tasks of identifying and segmenting those objects is captured by the notion of OoD segmentation [Chan et al., 2021a, Maag et al., 2022].

The recent contributions to the emerging field of OoD segmentation are mostly focused on OoD training, i.e., the incorporation of additional training data (not necessarily from the real world), sometimes obtained by large reconstruction models [Biase et al., 2021, Lis et al., 2019]. Another line of research is the use of uncertainty quantification methods such as Bayesian models [Mukhoti and Gal, 2018] or maximum softmax probability [Hendrycks and Gimpel, 2016]. Gradient-based uncertainties are considered for OoD detection in the classification task by Oberdiek et al. [2018], Huang et al. [2021] and Lee et al. [2022] and up to now, have not been applied to OoD segmentation. Grathwohl et al. [2020] show that gradient norms perform well in discriminating between in- and out-of-distribution. Moreover, gradient-based features are studied by Riedlinger et al. [2023] for object detection to estimate the prediction quality. Hornauer and Belagiannis [2022] investigate loss gradients w.r.t. feature activations in monocular depth estimation and show correlations of gradient magnitude with depth estimation accuracy.

In this work, we introduce a new method for uncertainty quantification in semantic segmentation and OoD segmentation based on gradient information. Magnitude features of gradients can be computed at inference time and provide information about the uncertainty propagated in the corresponding forward pass. These features represent pixel-wise uncertainty scores applicable to prediction quality estimation and OoD segmentation. An exemplary gradient uncertainty heatmap can be found in Figure 1 (bottom). Such uncertainty scores have shown improved performance for the quality estimation task in image classification compared to uncertainties contained in the softmax output of DNNs [Oberdiek et al., 2018]. In addition, instance-wise gradient uncertainty outperforms sampling methods like Monte-Carlo (MC) Dropout [Gal and Ghahramani, 2016] and Ensembles [Lakshminarayanan et al., 2017] in object detection [Riedlinger et al., 2023]. Calculating gradient uncertainty scores does not require any re-training of the DNN or computationally expensive sampling. Instead, only one backpropagation step for the gradients with respect to the final convolutional network layer is performed per inference to produce gradient scores. Note, that more than one backpropagation step can be performed if deeper gradients need to be computed and other parameters of the model are considered. An overview of our approach is shown in Figure 2.

An application to dense predictions such as semantic segmentation has escaped previous research. Single backpropagation steps per pixel on high-resolution input images quickly become infeasible given that 10^6 gradients have to be calculated. To overcome this issue, we present a new

approach to exactly compute the pixel-wise gradient scores in a batched and parallel manner applicable to a large class of segmentation architectures. We use these gradient scores to estimate the model uncertainty on pixel-level and also the prediction quality on segment-level. Segments are connected components of pixels belonging to the same class predicted by the semantic segmentation network. Finally, the gradient uncertainty heatmaps are investigated for OoD segmentation where high uncertainties indicate possible OoD objects.

We only assume a pre-trained semantic segmentation network as our method is applicable to a wide range of architectures. In our tests, we employ a state-of-the-art segmentation network [Chen et al., 2018] trained on Cityscapes [Cordts et al., 2016] evaluating in-distribution uncertainty estimation and on four OoD segmentation datasets, namely LostAndFound [Pinggera et al., 2016], Fishyscapes [Blum et al., 2019a], RoadAnomaly21 and RoadObstacle21 [Chan et al., 2021a], demonstrating OoD detection performance. The source code of our method is publicly available at <https://github.com/tobiasriedlinger/uncertainty-gradients-seg>. Our contributions are summarized as follows:

- We introduce a new method for uncertainty quantification in semantic segmentation. Our gradient-based approach is applicable to a wide range of segmentation architectures.
- For the first time, we show an efficient way of computing gradients in semantic segmentation on the pixel-level in a parallel manner making our method less computationally expensive than sampling-based methods.
- For the first time, we demonstrate the robustness of gradient-based uncertainty quantification with respect to predictive error detection and OoD segmentation. For the OoD segmentation task, we achieve area under precision-recall curve values of up to 69.3% on the LostAndFound benchmark outperforming a variety of methods that have substantially larger requirements.

The paper is structured as follows. We discuss the related work on uncertainty quantification and OoD segmentation in section 2. In section 3, we introduce our method of computing pixel-wise gradient uncertainty scores. Numerical results are shown in section 4, followed by concluding remarks in section 5.

2 RELATED WORK

2.1 UNCERTAINTY QUANTIFICATION

Bayesian approaches [MacKay, 1992] are widely used to estimate model uncertainty. The well-known approximation, MC Dropout [Gal and Ghahramani, 2016], has proven to be practically efficient in uncertainty estimation and is also

applied to semantic segmentation [Lee et al., 2020]. In addition, this method is considered to filter out predictions with low reliability [Wickstrøm et al., 2019]. Blum et al. [2019a] benchmarked pixel-wise uncertainty estimation methods based on Bayesian models or the network’s softmax output. Hoebel et al. [2020] extracted uncertainty information on pixel-level by using the maximum softmax probability and MC Dropout. Prediction quality evaluation approaches are introduced by DeVries and Taylor [2018] and Huang et al. [2016] working on single objects per image. These methods are based on additional CNNs acting as post-processing mechanism. Rottmann et al. [2020] present the concepts of meta classification (false positive detection) and meta regression (performance estimation) on segment-level using features as input extracted from the segmentation network’s softmax output. This line of research has been extended by a temporal component [Maag et al., 2020] and transferred to object detection [Schubert et al., 2021, Riedlinger et al., 2023] as well as to instance segmentation [Maag et al., 2021, Maag, 2021].

While MC Dropout as a sampling approach is computationally expensive to create pixel-wise uncertainties, our method computes only the gradients of the last layer during a single inference run and can be applied to a wide range of semantic segmentation networks without architectural changes. Compared with the work by Rottmann et al. [2020], our gradient information can extend the features extracted from the segmentation network’s softmax output to enhance the segment-wise quality estimation.

2.2 OOD SEGMENTATION

Uncertainty quantification methods demonstrate high uncertainty for erroneous predictions, so they can intuitively serve for OoD detection as well. For instance, this can be accomplished via maximum softmax (probability) [Hendrycks and Gimpel, 2016], MC Dropout [Mukhoti and Gal, 2018] or ensembles [Lakshminarayanan et al., 2017] which capture model uncertainty by averaging predictions over multiple sets of parameters. Another line of research is OoD detection training, relying on the exploitation of additional training data, not necessarily from the real world, but disjoint from the original training data [Besnier et al., 2021, Blum et al., 2019b, Chan et al., 2021b, Grcic et al., 2022, Tian et al., 2022]. In this regard, an external reconstruction model followed by a discrepancy network are considered by Biase et al. [2021], Lis et al. [2019], Lis et al. [2020] and Vojir et al. [2021] and normalizing flows are leveraged by Blum et al. [2019b] and Grcic et al. [2021]. Liang et al. [2018] as well as Lee et al. [2018] perform small adversarial perturbations on the input images to improve the separation of in- and out-of-distribution samples.

Specialized training approaches for OoD detection are based on different kinds of re-training with additional data and

often require generative models. Meanwhile, our method does not require OoD data, re-training or complex auxiliary models. Moreover, we do not run a full backward pass as is required for the computation of adversarial samples. In fact we found that it is often sufficient to only compute the gradients of the last convolutional layer. Our method is more related to classical uncertainty quantification approaches like maximum softmax, MC Dropout and ensembles. Note that the latter two are based on sampling and thus, much more computationally expensive compared to single inference.

3 METHOD DESCRIPTION

In the following, we consider a neural network with parameters θ yielding classification probabilities

$$\hat{\pi}(x, \theta) = (\hat{\pi}_1, \dots, \hat{\pi}_C) \quad (1)$$

over C semantic categories when presented with input x . During training on paired data (x, y) where $y \in \{1, \dots, C\}$ is the semantic label given to x , such a model is commonly trained by minimizing some kind of loss function \mathcal{L} between y and the predicted probability distribution $\hat{\pi}(x, \theta)$ using gradient descent on θ . The gradient step $\nabla_{\theta} \mathcal{L}(\hat{\pi}(x, \theta) \| y)$ then indicates the direction and strength of training feedback obtained by (x, y) . Asymptotically (in the amount of data and training steps taken), the expectation

$$\mathbb{E}_{(X, Y) \sim P} [\nabla_{\theta} \mathcal{L}(\hat{\pi}(X, \theta) \| Y)] \quad (2)$$

of the gradient w.r.t. the data generating distribution P will vanish since θ sits at a local minimum of \mathcal{L} . We assume, that strong models which achieve high test accuracy can be seen as an approximation of such a parameter configuration θ . Such a model has small gradients on in-distribution data which is close to samples (x, y) in the training data. Samples that differ from training data will receive larger feedback. Like-wise, we assume large training gradients from OoD samples that are far away from the effective support of P .

In order to quantify uncertainty about the prediction $\hat{\pi}(x, \theta)$, we replace the label y from above by some auxiliary label for which we make two concrete choices in our method. On the one hand, we replace y by the class prediction one-hot vector $y_k^{oh} = \delta_{k\hat{c}}$ with $\hat{c} = \arg \max_{k=1, \dots, C} \hat{\pi}_k$ and the Kronecker symbol δ_{ij} . This quantity correlates strongly with training labels on in-distribution data. On the other hand, we regard a uniform, all-warm label $y_k^{uni} = 1/C$ for $k = 1, \dots, C$ as a replacement for y . To motivate the latter choice, we consider that classification models are oftentimes trained on the categorical cross entropy loss

$$\mathcal{L}(\hat{\pi} \| y) = - \sum_{k=1}^C y_k \log(\hat{\pi}_k). \quad (3)$$

Since the gradient of this loss function is linear in the label y , a uniform choice will return the average gradient per class

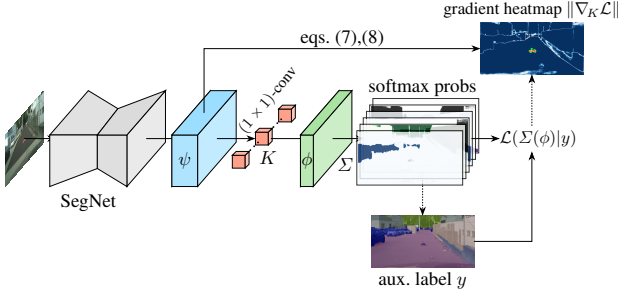


Figure 2: Schematic illustration of the computation of pixel-wise gradient norms for a semantic segmentation network with a final (1×1) -convolution. Auxiliary labels may be derived from the softmax prediction or supplied in any other way (e.g., as a uniform all-warm label). We circumvent direct back propagation per pixel by utilizing eqs. (7), (8).

which should be high on OoD data where all possible labels are similarly unlikely. The magnitude of $\nabla_{\theta} \mathcal{L}(\hat{\pi}|y)$ serves as uncertainty / OoD score. In the following, we explain how to compute such scores for pixel-wise classification models.

3.1 EFFICIENT COMPUTATION IN SEMANTIC SEGMENTATION

We regard a generic segmentation architecture utilizing a final convolution as the pixel-wise classification mechanism. In the following, we also assume that the segmentation model is trained via the commonly-used pixel-wise cross entropy loss $\mathcal{L}_{ab}(\phi(\theta)|y)$ (cf. eq. (3)) over each pixel (a, b) with feature map activations $\phi(\theta)$. Pixel-wise probabilities are obtained by applying the softmax function Σ to each output pixel, i.e., $\hat{\pi}_{ab,k} = \Sigma^k(\phi_{ab}(\theta))$. With eq. (3), we find for the loss gradient

$$\nabla_{\theta} \mathcal{L}_{ab}(\Sigma(\phi(\theta))|y) = \sum_{k=1}^C \Sigma^k(\phi_{ab})(1 - y_k) \cdot \nabla_{\theta} \phi_{ab}^k(\theta). \quad (4)$$

Here, θ is any set of parameters within the neural network. Detailed derivations of this and the following formulas of this section are provided in Appendix A. Here, ϕ is the convolution result of a pre-convolution feature map ψ (see Figure 2) against a filter bank K which assumes the role of θ . K has parameters $(K_e^h)_{fg}$ where e and h indicate in- and out-going channels respectively and f and g index the spatial filter position. The features ϕ are linear in both, K and ψ , and depend on bias parameters β in the form

$$\phi_{ab}^d = (K * \psi)_{ab}^d + \beta^d = \sum_{j=1}^{\kappa} \sum_{p,q=-s}^s (K_j^d)_{pq} \psi_{a+p,b+q}^j + \beta^d. \quad (5)$$

We denote by κ the total number of in-going channels and s is the spatial extent to either side of the filter K_j^d which has

total size $(2s + 1) \times (2s + 1)$. Explicitly for the last layer gradients we find

$$\frac{\partial \phi_{ab}^d}{\partial (K_e^h)_{fg}} = \delta_{dh} \psi_{a+f,b+g}^e. \quad (6)$$

Together with eq. (4), we obtain an explicit formula for computing the correct backpropagation gradients of the loss on pixel-level for our choices of auxiliary labels which we state in the following paragraph. The computation of the loss gradient can be traced in Figure 2.

If we take the predicted class \hat{c} as a one-hot label per pixel as auxiliary labels, i.e., y^{oh} , we obtain for the last layer gradients

$$\frac{\partial \mathcal{L}_{ab}(\Sigma(\phi)|y^{oh})}{\partial K_e^h} = \Sigma^h(\phi_{ab}) \cdot (1 - \delta_{h\hat{c}}) \cdot \psi_{ab}^e \quad (7)$$

which depends on quantities that are easily accessible during a forward pass through the network. Note, that the filter bank K for (1×1) -convolutions does not require spatial indices which is a common situation in segmentation networks. Similarly, we find for the uniform label $y_j^{umi} = 1/C$

$$\frac{\partial \mathcal{L}_{ab}(\Sigma(\phi)|y^{umi})}{\partial K_e^h} = \frac{C-1}{C} \Sigma^h(\phi_{ab}) \psi_{ab}^e. \quad (8)$$

Therefore, pixel-wise gradient norms are simple to implement and particularly efficient to compute for the last layer of the segmentation model. In the subsection A.2, we cover formulas for the more general case of deeper gradients as well.

3.2 UNCERTAINTY SCORES

We obtain pixel-wise scores (still depending on a and b) by computing the partial norm $\|\nabla_K \mathcal{L}_{ab}\|_p$ of this tensor over the indices e and h for some fixed value of p . This can again be done in a memory efficient way by the natural decomposition $\partial \mathcal{L} / \partial K_e^h = S^h \cdot \psi^e$. In addition to their use in error detection, these scores can be used in order to detect OoD objects in the input, i.e., instances of categories not present in the training distribution of the segmentation network. We identify OoD regions with pixels that have a gradient score higher than some threshold and find connected components like the one shown in Figure 1 (bottom). Different values of p are studied in the supplementary material. We also consider values $0 < p < 1$ in addition to positive integer values. Note, that such choices do not strictly define the geometry of a vector space norm, however, $\|\cdot\|_p$ may still serve as a notion of magnitude and generates a partial ordering. The tensorized multiplications required in eqs. (7) and (8) are far less computationally expensive than a forward pass through the DNN. This means that computationally, this method is preferable over prediction sampling like MC Dropout or ensembles. We abbreviate our method using

the pixel-wise gradient norms obtained from eqs. (7) and (8) by PGN_{oh} and PGN_{uni} , respectively. The particular value of p is denoted by superscript, e.g., $\text{PGN}_{oh}^{p=0.3}$ for the ($p = 0.3$)-seminorm of gradients obtained from y^{oh} .

4 EXPERIMENTS

In this section, we present the experimental setting first and then evaluate the uncertainty estimation quality of our method on pixel and segment level. Last, we apply our gradient-based method to OoD segmentation and show some visual results.

4.1 EXPERIMENTAL SETTING

Datasets We perform our tests on the Cityscapes [Cordts et al., 2016] dataset for semantic segmentation in street scenes and on four OoD segmentation datasets, i.e., LostAndFound [Pinggera et al., 2016], Fishyscapes [Blum et al., 2019a], RoadAnomaly21 and RoadObstacle21 [Chan et al., 2021a]¹. The Cityscapes dataset consists of 2,975 training and 500 validation images of dense urban traffic in 18 and 3 different German towns, respectively. The LostAndFound dataset contains 1,203 validation images with annotations for the road surface and the OoD objects, i.e., small obstacles on German roads in front of the ego-car. In [Chan et al., 2021a] this dataset is filtered (LostAndFound test-NoKnown) as children and bicycles are considered as OoD objects, although they are included in the Cityscapes training set. The Fishyscapes LostAndFound dataset is based on the LostAndFound dataset and refines the pixel-wise annotations, i.e., it is distinguished between OoD objects, background (Cityscapes classes) and void (anything else). Moreover frames that do not contain OoD objects as well as sequences with children and bikes are removed resulting in 100 validation images (and 275 non-public test images). The RoadObstacle21 dataset (412 test images) is comparable to the LostAndFound dataset as all obstacles appear on the road. However, the RoadObstacle21 dataset contains more diversity in the OoD objects as well as in the situations (night, snowy conditions and dirty roads) compared to the LostAndFound dataset where all sequences are recorded under good weather conditions. In the RoadAnomaly21 dataset the objects (anomalies) appear anywhere on the image which makes it comparable to the Fishyscapes LostAndFound dataset. While the latter dataset consists of frames extracted from a small number of different scenes, every image of the RoadAnomaly21 dataset (100 test images) shows a unique scene and a wider variety of anomalous objects.

Segmentation Networks We consider a state-of-the-art DeepLabv3+ network [Chen et al., 2018] with two different

Table 1: Pixel-wise uncertainty evaluation results for both backbone architectures and the Cityscapes dataset in terms of ECE and AuSE.

	WideResNet		SEResNeXt	
	ECE ↓	AuSE ↓	ECE ↓	AuSE ↓
Maximum Softmax	0.0017	<u>0.0277</u>	0.0032	0.0327
Entropy	0.0063	0.0642	0.0066	0.0623
$\text{PGN}_{oh}^{p=2}$ (ours)	<u>0.0019</u>	0.0268	<u>0.0039</u>	<u>0.0365</u>
$\text{PGN}_{uni}^{p=0.1}$ (ours)	0.0186	0.0784	0.0346	0.0427

backbones, WideResNet38 [Wu et al., 2016] and SEResNeXt50 [Hu et al., 2018]. The network with each respective backbone is trained on Cityscapes achieving a mean IoU value of 90.58% for the WideResNet38 backbone and 80.76% for the SEResNeXt50 on the Cityscapes validation set. We use one and the same model trained exclusively on the Cityscapes dataset for both tasks, the uncertainty estimation and the OoD segmentation, as our method does not need to be re-trained on OoD data. Therefore, our method leaves the entire segmentation performance of the base model completely intact.

4.2 NUMERICAL RESULTS

In our experiments, we apply different p -norms, $p \in \{0.1, 0.3, 0.5, 1, 2\}$, to our calculated gradients, see subsection 3.2. As we provide only a selection of results in the following, we refer to Appendix D for an ablation study on different values for p and to Appendix E for further results where the gradients of deeper layers are computed.

Pixel-wise Uncertainty Evaluation In order to assess the correlation of uncertainty and prediction errors on the pixel level, we resort to the commonly used sparsification graphs [Ilg et al., 2018]. Sparsification graphs normalized w.r.t. the optimal oracle (sparsification error) can be compared in terms of the so-called area under the sparsification error curve (AuSE). The closer the uncertainty estimation is to the oracle in terms of Brier score evaluation, i.e., the smaller the AuSE, the better the uncertainty eliminates false predictions by the model.

The AuSE metric is capable of grading the uncertainty ranking, however, does not address the statistics in terms of given confidence. Therefore, we resort to an evaluation of calibration in terms of expected calibration error (ECE, [Guo et al., 2017]) to assess the statistical reliability of the uncertainty measure.

As baseline methods we consider quantities that can be obtained without modifying the segmentation model (like MC Dropout) or retraining (like deep ensembles) and which do not need additional data (like re-calibration confidences). Our choices fall on the uncertainty ranking provided by the maximum softmax probabilities native to the segmentation

¹ Benchmark: (<http://segmentmeifyoucan.com/>)

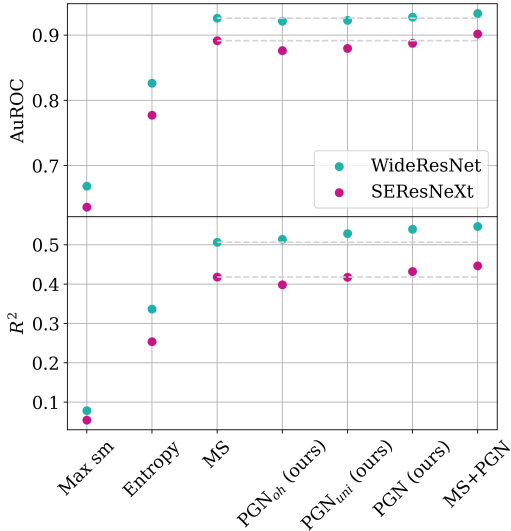


Figure 3: Segment-wise uncertainty evaluation results for both backbone architectures and the Cityscapes dataset in terms of classification AuROC and regression R^2 values. From left to right: maximum softmax, mean entropy, MetaSeg (MS) approach, gradient features obtained by predictive one-hot labels (PGN_{oh}), gradient features obtained by uniform labels (PGN_{uni}), all gradient features in combination (PGN), MetaSeg in combination with our gradient features.

model as well as the softmax entropy. An evaluation of calibration errors requires normalized scores, so we will normalize our gradient scores according to the highest value obtained on the test data for the computation of ECE.

The resulting metrics are compiled in Table 1 for both architectures evaluated on the Cityscapes val split. We see that both, the uncertainty ranking and the calibration of PGN_{oh} are roughly on par with the stronger maximum softmax baseline. Generally, we see the trend that PGN_{uni} has higher calibration error by one order of magnitude and higher sparsification errors of up to 5.2 percentage points (pp) which may indicate that this kind of score is less indicative of in-distribution errors. Note, that although there is no immediate reason for PGN_{oh} to be calibrated in any way, we find calibration errors that are competitive on pixel-level with those of the maximum softmax.

Segment-wise Prediction Quality Estimation To reduce the number of false positive predictions and to estimate the prediction quality, we use meta classification and meta regression introduced by [Rottmann et al., 2020]. As input for the post-processing models, the authors use information from the network’s softmax output which characterize uncertainty and geometry of a given segment like the segment size. The degree of randomness in semantic segmentation prediction is quantified by pixel-wise quantities, like entropy

and probability margin. To obtain segment-wise features from these quantities, they are aggregated over segments via average pooling. These features used in [Rottmann et al., 2020] serve as a baseline in our tests (called MetaSeg).

Similarly, we construct segment-wise features from our pixel-wise gradient p -norms for $p \in \{0.1, 0.3, 0.5, 1, 2\}$. We compute the mean and the variance of these pixel-wise values over a given segment. These features per segment are considered also for the inner and the boundary since the gradient scores may be higher on the boundary of a segment, see Figure 1 (bottom). The inner of the segment consists of all pixels whose eight neighboring pixels are also elements of the same segment. Furthermore, we define some relative mean and variance features over the inner and boundary which characterizes the degree of fractality. These hand-crafted quantities form a structured dataset where the columns correspond to features and the rows to predicted segments which serve as input to the post-processing models. Details on the construction of these features can be found in Appendix B.

We determine the prediction accuracy of semantic segmentation networks with respect to the ground truth via the segment-wise intersection over union (IoU, [Jaccard, 1912]). On the one hand, we perform the direct prediction of the IoU (meta regression) which serves as prediction quality estimate. On the other hand, we discriminate between $\text{IoU} = 0$ (false positive) and $\text{IoU} > 0$ (true positive) (meta classification). We use linear classification and regression models.

For the evaluation, we use AuROC (area under the receiver operating characteristic) for meta classification and the determination coefficient R^2 for meta regression. As baselines, we employ the maximum softmax probability [Hendrycks and Gimpel, 2016], the entropy and the MetaSeg framework. A comparison of these methods and our approach for the Cityscapes dataset is given in Figure 3. For the evaluation, we separate the gradient features obtained by one-hot (PGN_{oh}) and by uniform (PGN_{uni}) labels. Also, we consider using all gradient features (PGN) as input to the meta models. With PGN, we outperform the maximum softmax and the entropy baselines as well as the MetaSeg performance with the only exception of meta classification for the SEResNeXt backbone where MetaSeg achieves a marginal 0.41 pp higher AuROC value than ours. Moreover, we enhance the MetaSeg performance for both networks and both tasks combining the MetaSeg features with PGN by up to 1.02 pp for meta classification and up to 3.98 pp for meta regression. This indicates that gradient features contain information which is orthogonal to the information contained in the softmax output. In particular, the highest AuROC value of 93.31% achieved for the WideResNet backbone, shows the capability of our approach to estimate the prediction quality and filter out false positive predictions on the segment-level.

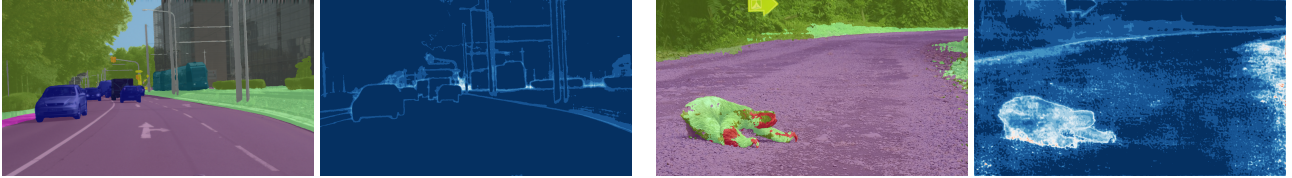


Figure 4: Semantic segmentation prediction and our gradient uncertainty heatmap ($\text{PGN}_{uni}^{p=0.5}$) for the Cityscapes dataset (left) and the RoadAnomaly21 dataset (right) for the WideResNet backbone.

Table 2: OoD segmentation results for the LostAndFound and the RoadObstacle21 dataset.

	LostAndFound test-NoKnown					RoadObstacle21				
	AuPRC \uparrow	FPR ₉₅ \downarrow	sIoU \uparrow	PPV \uparrow	$\overline{F_1}$ \uparrow	AuPRC \uparrow	FPR ₉₅ \downarrow	sIoU \uparrow	PPV \uparrow	$\overline{F_1}$ \uparrow
Ensemble	2.9	82.0	6.7	7.6	2.7	1.1	77.2	8.6	4.7	1.3
MC Dropout	36.8	35.6	17.4	34.7	13.0	4.9	50.3	5.5	5.8	1.1
Maximum Softmax	30.1	33.2	14.2	62.2	10.3	15.7	16.6	19.7	15.9	6.3
Entropy	52.0	30.0	40.4	53.8	42.4	20.6	16.3	21.4	19.5	10.4
$\text{PGN}_{oh}^{p=0.5}$	64.9	18.4	48.3	50.0	46.9	18.8	14.8	22.1	16.5	9.2
$\text{PGN}_{uni}^{p=0.5}$	69.3	9.8	50.0	44.8	45.4	16.5	19.7	19.5	14.8	7.4

OoD Segmentation Our results in OoD segmentation are based on the evaluation protocol of the SegmentMeIfYouCan benchmark [Chan et al., 2021a]. Evaluation on the pixel-level involves the threshold-independent area under precision-recall curve (AuPRC) and the false positive rate at the point of 0.95 true positive rate (FPR₉₅). The latter constitutes an interpretable choice of operating point for each method where a minimum true positive fraction is dictated. On segment-level, an adjusted version of the mean intersection over union (sIoU) which represents the accuracy of the segmentation obtained by thresholding at a particular point, positive predictive value (PPV or Precision) playing the role of binary instance-wise accuracy and the F_1 -score. The latter segment-wise metrics are averaged over thresholds between 0.25 and 0.75 with a step size of 0.05 leading to the quantities $\overline{\text{sIoU}}$, $\overline{\text{PPV}}$ and $\overline{F_1}$.

In contrast to the previous evaluations on predictive errors, we do not report here results for both of our models, rather we compare gradient scores as an OoD score as such against other methods on the benchmark and report the best result obtained for both, PGN_{oh} and PGN_{uni} . As baselines, we include the same methods as for error detection before since these constitute a reasonable comparison in addition to some of the well-established methods of estimating epistemic uncertainty like MC Dropout and deep ensemble. Note, that the standard entropy baseline is not featured in the official leaderboard, so we report our own results obtained by the softmax entropy with the WideResNet backbone which performed better. We include a full table of methods in Appendix C and find that our method is in several cases competitive with some of the stronger methods utilizing adversarial examples, auxiliary data or significant alterations of the model architecture.

The results verified by the official benchmark are com-

piled in Table 2 and Table 3. Across the board, PGN shows strong performance, almost exclusively delivering the best or second-best results with few exceptions. The only prominent exception is in the segment-based PPV metric on LostAndFound test-NoKnown where both, PGN_{oh} and PGN_{uni} come in behind the maximum softmax and entropy baseline. Meanwhile, the segmentation accuracy in terms of sIoU, as well as the F_1 score which is the harmonic mean of Recall and Precision are far superior to these two baselines. This indicates still better OoD segmentation quality and in particular better Recall achieved by PGN. Gradient scores perform perhaps the least convincingly on the RoadObstacle21 benchmark, where in three cases only the second-best performance is achieved. Overall however, we conclude strong performance of our method in terms of out-of-distribution segmentation across different datasets. We find a slight trend of PGN_{oh} performing better in the Obstacle track which can be seen to be closer to in-distribution data in semantic segmentation for autonomous driving. This connection would be consistent with our finding in actual in-distribution errors, while PGN_{uni} performs better on the Anomaly track which is more clearly out-of-distribution for street scene recognition. In several cases, our method even beats some of the stronger OoD segmentation methods utilizing, for example on RoadAnomaly21, adversarial samples (ODIN/Mahalanobis by over 9 pp in AuPRC), OoD data (Void Classifier by over 6 pp AuPRC) or generative models (JSRNet/Embedding Density by over 5 pp AuPRC and Image Resynthesis by over 10 pp in $\overline{\text{PPV}}$).

Figure 4 shows segmentation predictions of the pre-trained DeepLabv3+ network with the WideResNet38 backbone together with its corresponding $\text{PGN}_{uni}^{p=0.5}$ -heatmap. The two panels on the left show an in-distribution prediction on Cityscapes where uncertainty is mainly concentrated around segmentation boundaries which are always subject to high

Table 3: OoD segmentation results for the Fishyscapes LostAndFound and the RoadAnomaly21 dataset.

	Fishyscapes LostAndFound					RoadAnomaly21				
	AuPRC \uparrow	FPR ₉₅ \downarrow	sIoU \uparrow	PPV \uparrow	$\overline{F_1}$ \uparrow	AuPRC \uparrow	FPR ₉₅ \downarrow	sIoU \uparrow	PPV \uparrow	$\overline{F_1}$ \uparrow
Ensemble	0.3	90.4	3.1	1.1	0.4	17.7	91.1	16.4	20.8	3.4
MC Dropout	14.4	47.8	4.8	18.1	4.3	28.9	69.5	20.5	17.3	4.3
Maximum Softmax	5.6	40.5	3.5	9.5	1.8	28.0	72.1	15.5	15.3	5.4
Entropy	14.0	39.3	8.0	17.5	7.7	31.6	71.9	15.7	18.4	4.2
PGN ^{oh} _{p=0.5}	<u>22.8</u>	35.5	<u>12.1</u>	<u>27.3</u>	<u>14.1</u>	<u>39.3</u>	<u>66.5</u>	<u>23.1</u>	<u>21.5</u>	7.8
PGN ^{uni} _{p=0.5}	26.9	<u>36.6</u>	14.8	29.6	16.5	42.8	56.4	25.8	21.8	9.7

prediction uncertainty. Moreover, we see some false predictions in the far distance around the street crossing which can be found as a region of high gradient norm in the heatmap. In the two panels to the right, we see an OoD prediction from the RoadAnomaly21 dataset of a sloth crossing the street which is classified as part vegetation, terrain and person. The outline of the segmented sloth can be seen brightly in the gradient norm heatmap to the right indicating clear separation.

Limitations While our method performs well in terms of segment-wise error detection and raises accuracy compared with previous methods, we declare that our method is merely on-par with other uncertainty quantification methods for pixel-level considerations. Moreover, there have been submissions to the SegmentMeIfYouCan benchmark which significantly outperform our method, however, due to the simplicity and flexibility of our method this comes at no surprise. Note, that there are some light architectural restrictions when it comes to our method in that it is required for the final layer to be a convolution.

5 CONCLUSION

In this work, we presented an efficient method of computing gradient uncertainty scores for a wide class of deep semantic segmentation models. Moreover, we appreciate a low computational cost associated with them. Our experiments show that large gradient norms obtained by our method statistically correspond to erroneous predictions already on the pixel-level and can be normalized such that they yield similarly calibrated confidence measures as the maximum softmax score of the model. On a segment-level our method shows considerable improvement in terms of error detection. Gradient scores can be utilized to segment out-of-distribution objects significantly better than any other softmax- or output-based method on the SegmentMeIfYouCan benchmark and has competitive results with a variety of methods, in several cases clearly outperforming all of them. We hope that our contributions in this work and the insights into the computation of pixel-wise gradient feedback for segmentation models will inspire future work in uncertainty quantification and pixel-wise loss analysis.

Acknowledgements

We thank Hanno Gottschalk and Matthias Rottmann for discussion and useful advice. This work is supported by the Ministry of Culture and Science of the German state of North Rhine-Westphalia as part of the KI-Starter research funding program. The research leading to these results is funded by the German Federal Ministry for Economic Affairs and Climate Action within the project “KI Delta Learning“ (grant no. 19A19013Q). The authors would like to thank the consortium for the successful cooperation. The authors gratefully acknowledge the Gauss Centre for Supercomputing e.V. www.gauss-centre.eu for funding this project by providing computing time through the John von Neumann Institute for Computing (NIC) on the GCS Supercomputer JUWELS at Jülich Supercomputing Centre (JSC).

References

- Victor Besnier, Andrei Bursuc, David Picard, and Alexandre Briot. Triggering failures: Out-of-distribution detection by learning from local adversarial attacks in semantic segmentation. In *IEEE/CVF International Conference on Computer Vision (ICCV)*, 2021.
- Giancarlo Di Biase, Hermann Blum, Roland Y. Siegwart, and César Cadena. Pixel-wise anomaly detection in complex driving scenes. *IEEE/CVF Conference on Computer Vision and Pattern Recognition (CVPR)*, pages 16913–16922, 2021.
- Hermann Blum, Paul-Edouard Sarlin, Juan Nieto, Roland Siegwart, and Cesar Cadena. Fishyscapes: A benchmark for safe semantic segmentation in autonomous driving. In *IEEE/CVF International Conference on Computer Vision (ICCV) Workshops*, 2019a.
- Hermann Blum, Paul-Edouard Sarlin, Juan I. Nieto, Roland Y. Siegwart, and César Cadena. The fishyscapes benchmark: Measuring blind spots in semantic segmentation. *International Journal of Computer Vision*, pages 3119 – 3135, 2019b.
- Robin Chan, Krzysztof Lis, Svenja Uhlemeyer, Hermann Blum, Sina Honari, Roland Siegwart, Pascal Fua, Mathieu

- Salzmann, and Matthias Rottmann. Segmentmeifyoucan: A benchmark for anomaly segmentation. In *Conference on Neural Information Processing Systems Datasets and Benchmarks Track*, 2021a.
- Robin Chan, Matthias Rottmann, and Hanno Gottschalk. Entropy maximization and meta classification for out-of-distribution detection in semantic segmentation. In *IEEE/CVF International Conference on Computer Vision (ICCV)*, 2021b.
- Liang-Chieh Chen, Yukun Zhu, George Papandreou, Florian Schroff, and Hartwig Adam. Encoder-decoder with atrous separable convolution for semantic image segmentation. In *European Conference on Computer Vision (ECCV)*, 2018.
- Marius Cordts, Mohamed Omran, Sebastian Ramos, Timo Rehfeld, Markus Enzweiler, Rodrigo Benenson, Uwe Franke, Stefan Roth, and Bernt Schiele. The cityscapes dataset for semantic urban scene understanding. In *IEEE Conference on Computer Vision and Pattern Recognition (CVPR)*, 2016.
- Terrance DeVries and Graham W. Taylor. Leveraging uncertainty estimates for predicting segmentation quality. 2018.
- Yarin Gal and Zoubin Ghahramani. Dropout as a bayesian approximation: Representing model uncertainty in deep learning. In *Proceedings of the 33rd International Conference on International Conference on Machine Learning*, volume 48, pages 1050–1059, 2016.
- Will Grathwohl, Kuan-Chieh Wang, Jörn-Henrik Jacobsen, David Duvenaud, Mohammad Norouzi, and Kevin Swersky. Your classifier is secretly an energy based model and you should treat it like one. *International Conference on Learning (ICLR)*, 2020.
- Matej Grcic, Petra Bevandić, and Sinisa Segvic. Dense anomaly detection by robust learning on synthetic negative data. 2021.
- Matej Grcic, Petra Bevandić, and Sinisa Segvic. Densehybrid: Hybrid anomaly detection for dense open-set recognition. In *European Conference on Computer Vision (ECCV)*, pages 500–517, 2022.
- Chuan Guo, Geoff Pleiss, Yu Sun, and Kilian Q Weinberger. On calibration of modern neural networks. In *International conference on machine learning*, pages 1321–1330. PMLR, 2017.
- Dan Hendrycks and Kevin Gimpel. A baseline for detecting misclassified and out-of-distribution examples in neural networks. 2016.
- Katharina Hoebel, Vincent Andrearczyk, Andrew Beers, Jay Patel, Ken Chang, et al. An exploration of uncertainty information for segmentation quality assessment. 2020.
- Julia Hornauer and Vasileios Belagiannis. Gradient-based uncertainty for monocular depth estimation. In *Computer Vision–ECCV 2022: 17th European Conference, Tel Aviv, Israel, October 23–27, 2022, Proceedings, Part XX*, pages 613–630. Springer, 2022.
- Jie Hu, Li Shen, and Gang Sun. Squeeze-and-excitation networks. 2018.
- C. Huang, Q. Wu, and F. Meng. Qualitynet: Segmentation quality evaluation with deep convolutional networks. In *2016 Visual Communications and Image Processing (VCIP)*, pages 1–4, 2016.
- Rui Huang, Andrew Geng, and Yixuan Li. On the importance of gradients for detecting distributional shifts in the wild. In *Neural Information Processing Systems (NeurIPS)*, 2021.
- Eddy Ilg, Ozgun Cicek, Silvio Galesso, Aaron Klein, Osama Makansi, Frank Hutter, and Thomas Brox. Uncertainty estimates and multi-hypotheses networks for optical flow. In *Proceedings of the European Conference on Computer Vision (ECCV)*, pages 652–667, 2018.
- Paul Jaccard. The distribution of the flora in the alpine zone. *New Phytologist*, 1912.
- Balaji Lakshminarayanan, Alexander Pritzel, and Charles Blundell. Simple and scalable predictive uncertainty estimation using deep ensembles. In *Neural Information Processing Systems (NeurIPS)*, page 6405–6416, 2017.
- Hong Lee, Seong Tae Kim, Nassir Navab, and Yong Ro. Efficient ensemble model generation for uncertainty estimation with bayesian approximation in segmentation. 2020.
- Jinsol Lee, Mohit Prabhushankar, and Ghassan Alregib. Gradient-based adversarial and out-of-distribution detection. In *International Conference on Machine Learning*, 2022.
- Kimin Lee, Kibok Lee, Honglak Lee, and Jinwoo Shin. A simple unified framework for detecting out-of-distribution samples and adversarial attacks. *Neural Information Processing Systems (NeurIPS)*, 2018.
- Shiyu Liang, Yixuan Li, and Rayadurgam Srikant. Enhancing the reliability of out-of-distribution image detection in neural networks. *International Conference on Learning (ICLR)*, 2018.
- Krzysztof Lis, Krishna Nakka, Pascal Fua, and Mathieu Salzmann. Detecting the unexpected via image resynthesis. In *IEEE/CVF International Conference on Computer Vision (ICCV)*, 2019.

- Krzysztof Lis, Sina Honari, Pascal Fua, and Mathieu Salzmann. Detecting road obstacles by erasing them. 2020.
- Kira Maag. False negative reduction in video instance segmentation using uncertainty estimates. In *IEEE International Conference on Tools with Artificial Intelligence (ICTAI)*, 2021.
- Kira Maag, Matthias Rottmann, and Hanno Gottschalk. Time-dynamic estimates of the reliability of deep semantic segmentation networks. In *IEEE International Conference on Tools with Artificial Intelligence (ICTAI)*, 2020.
- Kira Maag, Matthias Rottmann, Serin Varghese, Fabian Hüger, Peter Schlicht, and Hanno Gottschalk. Improving video instance segmentation by light-weight temporal uncertainty estimates. In *International Joint Conference on Neural Network (IJCNN)*, 2021.
- Kira Maag, Robin Chan, Svenja Uhlemeyer, Kamil Kowol, and Hanno Gottschalk. Two video data sets for tracking and retrieval of out of distribution objects. In *Asian Conference on Computer Vision (ACCV)*, pages 3776–3794, 2022.
- David J. C. MacKay. A practical bayesian framework for backpropagation networks. *Neural Computation*, 4(3): 448–472, 1992.
- Jishnu Mukhoti and Yarín Gal. Evaluating bayesian deep learning methods for semantic segmentation. 2018.
- Philip Oberdiek, Matthias Rottmann, and Hanno Gottschalk. Classification uncertainty of deep neural networks based on gradient information. *Artificial Neural Networks and Pattern Recognition (ANNPR)*, 2018.
- Peter Pinggera, Sebastian Ramos, Stefan Gehrig, Uwe Franke, Carsten Rother, and Rudolf Mester. Lost and found: detecting small road hazards for self-driving vehicles. In *IEEE/RSJ International Conference on Intelligent Robots and Systems (IROS)*, 2016.
- Tobias Riedlinger, Matthias Rottmann, Marius Schubert, and Hanno Gottschalk. Gradient-based quantification of epistemic uncertainty for deep object detectors. In *IEEE/CVF Winter Conference on Applications of Computer Vision (WACV)*, pages 3921–3931, 2023.
- Matthias Rottmann, Pascal Colling, Thomas-Paul Hack, Fabian Hüger, Peter Schlicht, et al. Prediction error meta classification in semantic segmentation: Detection via aggregated dispersion measures of softmax probabilities. In *IEEE International Joint Conference on Neural Networks (IJCNN) 2020*, 2020.
- Marius Schubert, Karsten Kahl, and Matthias Rottmann. Metadetect: Uncertainty quantification and prediction quality estimates for object detection. In *International Joint Conference on Neural Networks (IJCNN)*, 2021.
- Yu Tian, Yuyuan Liu, Guansong Pang, Fengbei Liu, Yuanhong Chen, and Gustavo Carneiro. Pixel-wise energy-biased abstention learning for anomaly segmentation on complex urban driving scenes. In *European Conference on Computer Vision (ECCV)*, 2022.
- Tomas Vojir, Tomáš Šipka, Rahaf Aljundi, Nikolay Chumerin, Daniel Olmeda Reino, and Jiri Matas. Road anomaly detection by partial image reconstruction with segmentation coupling. In *IEEE/CVF International Conference on Computer Vision (ICCV)*, pages 15651–15660, 2021.
- Jingdong Wang, Ke Sun, Tianheng Cheng, Borui Jiang, Chaorui Deng, Yang Zhao, D. Liu, Yadong Mu, Mingkui Tan, Xinggang Wang, Wenyu Liu, and Bin Xiao. Deep high-resolution representation learning for visual recognition. *IEEE Transactions on Pattern Analysis and Machine Intelligence*, 2021.
- Kristoffer Wickstrøm, Michael Kampffmeyer, and Robert Jenssen. Uncertainty and interpretability in convolutional neural networks for semantic segmentation of colorectal polyps. *Medical Image Analysis*, 60:101619, 2019.
- Zifeng Wu, Chunhua Shen, and Anton Hengel. Wider or deeper: Revisiting the resnet model for visual recognition. *Pattern Recognition*, 2016.
- Yi Zhu, Karan Sapra, Fitsum A Reda, Kevin J Shih, Shawn Newsam, Andrew Tao, and Bryan Catanzaro. Improving semantic segmentation via video propagation and label relaxation. In *Proceedings of the IEEE/CVF Conference on Computer Vision and Pattern Recognition*, pages 8856–8865, 2019.

APPENDIX

A COMPUTATIONAL DERIVATIONS AND IMPLEMENTATION DETAILS

A.1 COMPUTATIONS

In this work we assume that the final activation in the segmentation network is given by a softmax activation of categorical features ϕ in the last layer

$$\Sigma^j(\phi) = \frac{e^{\phi^j}}{\sum_{i=1}^C e^{\phi^i}} \quad (9)$$

where C is the number of classes and $\phi = \phi(\theta)$ is now dependent on a set of parameters θ . In order to compute the gradients of the categorical cross entropy at pixel (a, b) given any auxiliary label y

$$\mathcal{L}_{ab}(\phi(\theta)||y) = - \sum_{j=1}^C y_{ab,j} \log(\Sigma^j(\phi_{ab}(\theta))), \quad (10)$$

we require the derivative of the softmax function

$$\begin{aligned}
\nabla_{\theta} \Sigma^j(\phi(\theta)) &= \frac{e^{\phi^j} \nabla_{\theta} \phi^j}{\sum_{i=1}^C e^{\phi^i}} - \frac{e^{\phi^j} \sum_{k=1}^C e^{\phi^k} \nabla_{\theta} \phi^k}{\left(\sum_{i=1}^C e^{\phi^i}\right)^2} \\
&= \Sigma^j(\phi) \cdot \nabla_{\theta} \phi^j \sum_{k=1}^C \Sigma^k(\phi) \\
&\quad - \Sigma^j(\phi) \sum_{k=1}^C \Sigma^k(\phi) \cdot \nabla_{\theta} \phi^k \\
&= \Sigma^j(\phi) \left(\sum_{k=1}^C \Sigma^k(\phi) \cdot \nabla_{\theta} \phi^j - \Sigma^k \nabla_{\theta} \phi^k \right) \\
&= \Sigma^j(\phi) \sum_{k=1}^C \Sigma^k(\phi) (\delta_{kj} - 1) \nabla_{\theta} \phi^k.
\end{aligned} \tag{11}$$

Note, that the auxiliary label $y \in [0, 1]^C$ may be anything, e.g., actual ground truth information about pixel (a, b) , the predicted probability distribution at that location, the one-hot encoded prediction or a uniform class distribution. In the following, we regard y to be independent of ϕ . The gradient of the cross entropy loss is

$$\begin{aligned}
\nabla_{\theta} \mathcal{L}_{ab}(\phi(\theta) \| y) &= - \sum_{j=1}^C y_{ab,j} \frac{1}{\Sigma^j(\phi_{ab})} \nabla_{\theta} \Sigma^j(\phi_{ab}) \\
&= \sum_{j=1}^C \sum_{k=1}^C (y_{ab,j} \Sigma^k(\phi_{ab}) - y_j \Sigma^k(\phi_{ab}) \delta_{kj}) \\
&\quad \cdot \nabla_{\theta} \phi_{ab}^k(\theta) \\
&= \sum_{k=1}^C \Sigma^k(\phi_{ab}) (1 - y_k) \cdot \nabla_{\theta} \phi_{ab}^k(\theta)
\end{aligned} \tag{12}$$

The feature maps are the result of convolution $\mathcal{C}_{K,\beta}$ against a filter bank $K \in \mathbb{R}^{\kappa_{\text{in}} \times \kappa_{\text{out}} \times (2s+1) \times (2s+1)}$ and addition of a bias vector $\beta \in \mathbb{R}^{\kappa_{\text{out}}}$. Here, κ_{in} and κ_{out} denote the number of in- and out-going channels, respectively. K has parameters $(K_e^h)_{fg}$ where e and h indicate in- and out-going channels respectively and f and g index the spatial filter position. In particular, we obtain the value ϕ_{ab}^d at pixel location (a, b) in channel d by

$$\begin{aligned}
\phi_{ab}^d(K, \beta, \psi) &= [\mathcal{C}_{K,\beta}(\psi)]_{ab}^d = (K * \psi)_{ab}^d + \beta^d \\
&= \sum_{c=1}^{\kappa_{\text{in}}} \sum_{q=-s}^s \sum_{r=-s}^s (K_c^d)_{qr} \psi_{a+q,b+r}^c + \beta^d.
\end{aligned} \tag{13}$$

Here, we assume the filters of size $(2s+1) \times (2s+1)$ indexed symmetrically around their center and ψ is the feature map pre-convolution. Note, also that the bias is constant across the indices a and b . Taking explicit derivatives of this

expression with respect to one of the parameters in K yields

$$\begin{aligned}
\frac{\partial (K * \phi)_{ab}^d}{\partial (K_e^h)_{fg}} &= \sum_{c=1}^{\kappa_{\text{in}}} \sum_{q,r=-s}^s \frac{\partial (K_c^d)_{qr}}{\partial (K_e^h)_{fg}} \psi_{a+q,b+r}^c \\
&= \sum_{c=1}^{\kappa_{\text{in}}} \sum_{q,r=-s}^s \delta^{dh} \delta_{ce} \delta_{pf} \delta_{qg} \psi_{a+q,b+r}^c \\
&= \delta^{dh} \psi_{a+f,b+g}^e.
\end{aligned} \tag{14}$$

When utilizing the predicted one-hot vector (self-learning gradient), i.e., $y_k^{\phi^h} = \delta_{k\hat{c}}$ and using the fact that the last-layer convolution is (1×1) , we obtain

$$\begin{aligned}
\frac{\partial}{\partial K_e^f} \mathcal{L}_{ab} &= \sum_{k=1}^C \Sigma^k(\phi_{ab}) (1 - \delta_{k\hat{c}}) \frac{\partial \phi_{ab}^k}{\partial K_e^f} \\
&= \Sigma^f(\phi_{ab}) (1 - \delta_{f\hat{c}}) \psi_{ab}^e.
\end{aligned} \tag{15}$$

while the uniform categorical label $y_k = \frac{1}{C}$ yields

$$\begin{aligned}
\frac{\partial}{\partial K_e^f} \mathcal{L}_{ab} &= \sum_{k=1}^C \Sigma^k(\phi_{ab}) \left(1 - \frac{1}{C}\right) \cdot \nabla_{\theta} \phi_{ab}^k(\theta) \\
&= \frac{C-1}{C} \Sigma^f(\phi_{ab}) \psi_{ab}^e.
\end{aligned} \tag{16}$$

A.2 COMPUTING DEEPER GRADIENTS VIA EXPLICIT BACKPROPAGATION

While for the last-layer gradients the computation from above simplifies significantly due to the fact that pixel-wise gradients only depend on the feature map values at the same pixel-location. Deeper layers are usually not (1×1) , so the forward pass couples feature map values over a larger receptive field, e.g., (3×3) . However, gradients for the second-to-last layer can still be computed with moderate effort by extracting feature map patches via the unfold function. Here, we consider a DeepLabv3+ implementation² Zhu et al. [2019] for which the feature maps depend in the following way on the weights of the second-to-last layer $T-1$ (where T indicates the last layer):

$$\phi(K_{T-1}) = \mathcal{C}_{K_{T-1}, \beta_T} \circ \text{ReLU} \circ \text{BN}_T \circ \mathcal{C}_{K_{T-1}, \beta_{T-1}}(\psi_{T-1}), \tag{17}$$

where BN_T is a batch normalization layer and ψ_{T-1} are the features prior to the convolution $\mathcal{C}_{K_{T-1}, \beta_{T-1}}$ in question. With fully expanded indices, this amounts to

$$\begin{aligned}
\phi_{ab}^d &= \sum_{k_T} K_{k_T}^d \text{ReLU} \left(\text{BN}_T \left[\sum_{k_{T-1}} \sum_{q,r} \left((K_{T-1})_{k_{T-1}}^{k_T} \right)_{qr} \right. \right. \\
&\quad \left. \left. (\psi_{T-1})_{a+q,b+r}^{k_{T-1}} + \beta_{T-1}^{k_T} \right] \right) + \beta_T^d
\end{aligned} \tag{18}$$

²<https://github.com/NVIDIA/semantic-segmentation/tree/sdcnet>

with k_T, k_{T-1} indexing the respective amount of channels and q, r indexing the filter coordinates of K_{T-1} . Note, that we still assume here that the last convolutional layer has spatial extent 0 into both directions, so $K_T \in \mathbb{R}^{k_{in} \times C \times 1 \times 1}$. The chain rule for this forward pass is then

$$\begin{aligned} \frac{\partial \phi_{ab}^d}{\partial ((K_{T-1})_{gh}^f)} &= \sum_{k_T} K_{k_T}^d \text{ReLU}'(\cdot) \cdot \text{BN}'_T \cdot \\ &\cdot \left[\sum_{k_{T-1}} \sum_{q,r} \frac{\partial ((K_{T-1})_{k_{T-1}}^{k_T})_{qr}}{\partial ((K_{T-1})_{gh}^f)} (\psi_{T-1})_{a+q, b+r}^{k_{T-1}} \right] \\ &= \sum_{k_T} K_{k_T}^d \text{ReLU}'(\cdot) \cdot \text{BN}'_T \cdot \\ &\cdot \left[\sum_{k_{T-1}} \sum_{q,r} \delta^{k_T f} \delta_{k_{T-1} e} \delta_{gp} \delta_{hq} (\psi_{T-1})_{a+q, b+r}^{k_{T-1}} \right] \\ &= K_f^d (\text{ReLU}')_{ab}^f \cdot (\text{BN}'_T)_{ab}^f \cdot \\ &\cdot [(\psi_{T-1})_{a+g, b+h}^e] \end{aligned} \quad (19)$$

The term with the derivative of the ReLU activation is simply the Heaviside function evaluated at the features pre-activation which have been computed in the forward pass anyway (the discontinuity at zero has vanishing probability of an evaluation). The derivative of the batch normalization layer is multiplication by the linear batch norm parameter which is applied channel-wise. The running indices g and h only apply to the last factor which can be computationally treated by extracting (3×3) -patches from ψ_{T-1} using the unfold operation. In computing the norm of $\nabla_{K_{T-1}} \phi_{ab}^d$ with respect to the indices e, f, g and h , we note that the expression in eq. (19) is a product of two tensors $S_f \cdot \Psi_{gh}^e$ for each pixel (a, b) . L^p -norms of such tensors $T_{ij} = S_i \Psi_j$ factorize which makes their computation feasible:

$$\begin{aligned} \|T\|_p &= \left(\sum_{i,j} |T_{ij}|^p \right)^{\frac{1}{p}} = \left(\sum_{i,j} |S_i|^p |\Psi_j|^p \right)^{\frac{1}{p}} \\ &= \left(\sum_i \left[|S_i|^p \sum_j |\Psi_j|^p \right] \right)^{\frac{1}{p}} = \|S\|_p \|\Psi\|_p. \end{aligned} \quad (20)$$

B DETAILS ON THE FEATURE CONSTRUCTION FOR SEGMENT-WISE PREDICTION QUALITY ESTIMATION

The tasks of meta classification (false positive detection) and meta regression (prediction quality estimation) based on uncertainty measures extracted from the network’s softmax output were introduced in [Rottmann et al., 2020]. The neural network provides for each pixel z given an input image x a probability distribution $f_z(y|x)$ over a label space

$C = \{y_1, \dots, y_c\}$, with $y \in C$. The degree of randomness in the semantic segmentation prediction $f_z(y|x)$ is quantified by pixel-wise dispersion measures, like entropy

$$E_z(x) = -\frac{1}{\log(c)} \sum_{y \in C} f_z(y|x) \log f_z(y|x) \quad (21)$$

and probability margin

$$M_z(x) = 1 - f_z(\hat{y}_z(x)|x) + \max_{y \in C \setminus \{\hat{y}_z(x)\}} f_z(y|x) \quad (22)$$

where

$$\hat{y}_z(x) = \arg \max_{y \in C} f_z(y|x) \quad (23)$$

is the predicted class for each pixel z . To obtain segment-wise features from these dispersion measures which characterize uncertainty, they are aggregated over segments via average pooling obtaining mean dispersions μE and μM . As erroneous or poor predictions oftentimes have fractal segment shapes, it is distinguished between the inner of the segment (consisting of all pixels whose eight neighboring pixels are also elements of this segment) and the boundary. This results in segment size S and mean dispersion features per segment also for the inner (*in*) and the boundary (*bd*). Furthermore, relative segment sizes $\tilde{S} = S/S_{bd}$ and $\tilde{S}_{in} = S_{in}/S_{bd}$ as well as relative mean dispersions $\mu \tilde{D} = \mu D \tilde{S}$ and $\mu \tilde{D}_{in} = \mu D_{in} \tilde{S}_{in}$ where $D \in \{E, M\}$ are defined. Moreover, the mean class probabilities $P(y)$ for each class $y \in C$ are added resulting in the set of hand-crafted features

$$\begin{aligned} \{S, S_{in}, S_{bd}, \tilde{S}, \tilde{S}_{in}\} \cup \{P(y) : y = 1, \dots, c\} \\ \cup \{\mu D, \mu D_{in}, \mu D_{bd}, \mu \tilde{D}, \mu \tilde{D}_{in} : D \in \{E, M\}\}. \end{aligned} \quad (24)$$

These features serve as a baseline in our tests.

The computed gradients in section 3 with applied p -norm, $p \in \{0.1, 0.3, 0.5, 1, 2\}$, are denoted by $G_z^{p=\#}(x)$, $\# \in \{0.1, 0.3, 0.5, 1, 2\}$, for image x . Similar to the dispersion measures, we compute the mean and additionally the variance of these pixel-wise values of a given segment to obtain $\mu G^{p=\#}$ and $v G^{p=\#}$, respectively. Since the gradient uncertainties may be higher on the boundary of a segment, the mean and variance features per segment are considered also for the inner and the boundary. Furthermore, we define relative mean and variance features to quantify the degree of fractality. This results in the following gradient features

$$\begin{aligned} \{\mu G^{p=\#}, \mu G_{in}^{p=\#}, \mu G_{bd}^{p=\#}, \mu \tilde{G}^{p=\#}, \mu \tilde{G}_{in}^{p=\#}, \\ v G^{p=\#}, v G_{in}^{p=\#}, v G_{bd}^{p=\#}, v \tilde{G}^{p=\#}, v \tilde{G}_{in}^{p=\#} : \\ \# \in \{0.1, 0.3, 0.5, 1, 2\}\}. \end{aligned} \quad (25)$$

Note, these features can be computed for the gradient scores obtained from the predictive one-hot (PGN_{oh}) and the uniform label (PGN_{uni}) as well as for gradients of deeper layers (see subsection A.2).

C EXTENDED OOD SEGMENTATION RESULTS

In subsection 4.2, we have compared our approach with comparable uncertainty estimation methods such as entropy and maximum softmax. Moreover, we considered two sampling approaches, MC Dropout and ensembles, as baselines. In Table 4 and Table 5, we provide the comparison of our method with more methods from the benchmark. In detail, the first block consists of approaches using OoD data, i.e., Void Classifier [Blum et al., 2019b], SynBoost [Bise et al., 2021], Maximized Entropy [Chan et al., 2021b], PEBAL [Tian et al., 2022] and DenseHybrid [Grcic et al., 2022]. The methods of the second block use complex auxiliary/generative models, namely Image Resynthesis [Lis et al., 2019], Road Inpainting [Lis et al., 2020], embedding density [Blum et al., 2019b], NFlowJS [Grcic et al., 2021], JSRNet [Vojir et al., 2021] and ObsNet [Besnier et al., 2021]. The ODIN [Liang et al., 2018] and Mahalanobis [Lee et al., 2018] baselines (in the third block) perform adversarial attacks on the input images and thus, require a full and expensive backward pass. Per block we indicate the best method for each of the considered metrics.

We outperform the two latter baselines (ODIN and Mahalanobis) for the LostAndFound as well as the RoadAnomaly21 dataset. In detail, we obtain AuPRC values up to 22.8 pp higher on segment-level and \bar{F}_1 values up to 24.8 pp higher on pixel-level. For the other two datasets we achieve similar results. Furthermore, we beat the Void Classifier method, that uses OoD data during training, in most cases. We improve the AuPRC metric by up to 64.5 pp and the \bar{sIoU} metric by up to 48.2 pp, both for the LostAndFound dataset. In addition, our gradient norms outperform in most cases the Embedding Density approach which is based on normalizing flows. Summing up, we have shown superior OoD segmentation performance in comparison to the other uncertainty based methods (see subsection 4.2) and we outperform some of the more complex approaches (using OoD data, adversarial samples or generative models).

D ABLATION: DIFFERENT p -NORMS

In this section, we present an ablation study for different p -norms, $p \in \{0.1, 0.3, 0.5, 1, 2\}$, that are applied to the calculated gradients of the last convolutional layer.

Pixel-wise Uncertainty Evaluation The area under the sparsification error curve (AuSE) is considered to assess the correlation of uncertainty and prediction errors on pixel level and the expected calibration error (ECE) to assess the statistical reliability of the uncertainty measure. In Table 6 the results for the different p -norms in terms of these two metrics are given. We observe improved performance for the gradient scores obtained from the predictive one-hot label

with respect to both metrics. These scores are better calibrated for greater values of p , whereas there is no clear trend for the AuSE metric. In contrast, for the gradient scores obtained from the uniform label the calibration ability as well as the sparsification error enhance mostly for decreasing values of p .

Segment-wise Prediction Quality Estimation For the segment-wise prediction quality estimation, we consider meta classification, i.e., classifying between $IoU = 0$ (false positive) and $IoU > 0$ (true positive), and meta regression, i.e., direct prediction of the IoU. The gradient features (see eq. (25)) which are computed for each value of p , also separated for predictive one-hot and uniform labels, serve as input for the meta models. The results are given in Table 7 and visualized in Figure 5. The WideResNet backbone outperforms the SEResNeXt for meta classification and regression. Moreover, higher AuROC and R^2 performances are achieved for greater values of p independent of the architecture or the label (predictive one-hot or uniform) used for gradient scores computation.

OoD Segmentation Our approach provides pixel-wise uncertainty scores obtained by computing the partial norm. In Figure 6 the pixel-wise heatmaps for both backbones, different p -norms and the predictive one-hot as well as the uniform label are shown. We observe that for higher p values the number of uncertain pixels increases, the gradients are more sensitive to unconfident predictions. For a p value of 0.1 only a few pixels of OoD object have high uncertainty while the background is completely certain. For values of $p = 1$ and $p = 2$, in particular using the uniform label, the gradient scores show higher uncertainties in more sectors. To identify out-of-distribution regions, we threshold per pixel on our gradient scores, i.e., high uncertainty corresponds to out-of-distribution. Here, the OoD objects are mostly covered (and not so many background pixels) for p values of 0.3 and 0.5. These observations are reflected in the OoD segmentation results, given in Table 8 and Table 9.

For the LostAndFound dataset and the Fishyscapes LostAndFound dataset, the best results are achieved for the 0.3 and 0.5 p -norms. For the RoadAnomaly21 dataset, also for higher p values strong (in one case even the best) results are obtained. Across these three datasets, there is no favorability which backbone architecture or label (predictive one-hot or uniform) performs better. In comparison for the RoadObstacle21 dataset, the WideResNet backbone with gradient scores obtained from the predictive one-hot performs best.

In summary, there is no clear tendency which p -norm outperforms the others for the different tasks of pixel- and segment-wise uncertainty estimation as well as for OoD segmentation. However, there is a strong trend towards $p \in \{0.3, 0.5\}$ performing especially strongly.

Table 4: OoD segmentation results for the LostAndFound and the RoadObstacle21 dataset.

	LostAndFound test-NoKnown					RoadObstacle21				
	AuPRC \uparrow	FPR ₉₅ \downarrow	sIoU \uparrow	PPV \uparrow	$\overline{F_1}$ \uparrow	AuPRC \uparrow	FPR ₉₅ \downarrow	sIoU \uparrow	PPV \uparrow	$\overline{F_1}$ \uparrow
Void Classifier	4.8	47.0	1.8	35.1	1.9	10.4	41.5	6.3	20.3	5.4
SynBoost	81.7	4.6	36.8	72.3	48.7	71.3	3.2	44.3	41.8	37.6
Maximized Entropy	77.9	9.7	45.9	63.1	49.9	85.1	0.8	47.9	62.6	48.5
PEBAL	—	—	—	—	—	5.0	12.7	29.9	7.6	5.5
DenseHybrid	78.7	2.1	46.9	52.1	52.3	87.1	0.2	45.7	50.1	50.7
Image Resynthesis	57.1	8.8	27.2	30.7	19.2	37.7	4.7	16.6	20.5	8.4
Road Inpainting	82.9	35.8	49.2	60.7	52.3	54.1	47.1	57.6	39.5	36.0
Embedding Density	61.7	10.4	37.8	35.2	27.6	0.8	46.4	35.6	2.9	2.3
NFlowJS	89.3	0.7	54.6	59.7	61.8	85.6	0.4	45.5	49.5	50.4
JSRNet	74.2	6.6	34.3	45.9	36.0	28.1	28.9	18.6	24.5	11.0
ODIN	52.9	30.0	39.8	49.3	34.5	22.1	15.3	21.6	18.5	9.4
Mahalanobis	55.0	12.9	33.8	31.7	22.1	20.9	13.1	13.5	21.8	4.7
$\text{PGN}_{oh}^{p=0.5}$	64.9	18.4	48.3	50.0	46.9	18.8	14.8	22.1	16.5	9.2
$\text{PGN}_{uni}^{p=0.5}$	69.3	9.8	50.0	44.8	45.4	16.5	19.7	19.5	14.8	7.4

Table 5: OoD segmentation results for the Fishyscapes LostAndFound and the RoadAnomaly21 dataset.

	Fishyscapes LostAndFound					RoadAnomaly21				
	AuPRC \uparrow	FPR ₉₅ \downarrow	sIoU \uparrow	PPV \uparrow	$\overline{F_1}$ \uparrow	AuPRC \uparrow	FPR ₉₅ \downarrow	sIoU \uparrow	PPV \uparrow	$\overline{F_1}$ \uparrow
Void Classifier	11.7	15.3	9.2	39.1	14.9	36.6	63.5	21.1	22.1	6.5
SynBoost	64.9	30.9	27.9	48.6	38.0	56.4	61.9	34.7	17.8	10.0
Maximized Entropy	44.3	37.7	21.1	48.6	30.0	85.5	15.0	49.2	39.5	28.7
PEBAL	—	—	—	—	—	49.1	40.8	38.9	27.2	14.5
DenseHybrid	—	—	—	—	—	78.0	9.8	54.2	24.1	31.1
Image Resynthesis	5.1	29.8	5.1	12.6	4.1	52.3	25.9	39.7	11.0	12.5
Embedding Density	8.9	42.2	5.9	10.8	4.9	37.5	70.8	33.9	20.5	7.9
NFlowJS	—	—	—	—	—	56.9	34.7	36.9	18.0	14.9
JSRNet	—	—	—	—	—	33.6	43.9	20.2	29.3	13.7
ObsNet	—	—	—	—	—	75.4	26.7	44.2	52.6	45.1
ODIN	15.5	38.4	9.9	21.9	9.7	33.1	71.7	19.5	17.9	5.2
Mahalanobis	32.9	8.7	19.6	29.4	19.2	20.0	87.0	14.8	10.2	2.7
$\text{PGN}_{oh}^{p=0.5}$	22.8	35.5	12.1	27.3	14.1	39.3	66.5	23.1	21.5	7.8
$\text{PGN}_{uni}^{p=0.5}$	26.9	36.6	14.8	29.6	16.5	42.8	56.4	25.8	21.8	9.7

E ABLATION: DEEPER LAYERS

In subsection A.2, we have shown how to compute the gradients also for deeper layers than the last convolutional one. In this section, we discuss the numerical results for the second-to-last layer in comparison to the last.

Pixel-wise Uncertainty Evaluation The results for the pixel-wise uncertainty estimation measured by ECE and AuSE are given in Table 6 for both layers. For the gradient scores obtained from the predictive one-hot, the evaluation metrics are mainly similar showing only small performance gaps. The results differ for the uniform labels, although there is no trend to which layer achieves the higher ones.

Segment-wise Prediction Quality Estimation The segment-wise meta classification and regression results are shown in Table 7. We observe the same behavior for the second-to-last as for the last one, namely that as p increases, performance improves for both metrics. Furthermore, the performance is almost equal for the second-to-last and

the last layer for the 1 and the 2 norm independent of the backbone and labels to obtain the gradient scores.

OoD Segmentation In Table 10 the OoD segmentation results are given. In comparison to the performance of the gradient scores of the last layer (see Table 8 and Table 9), the performance of the second-to-last layer is poor, i.e., the results for all evaluation metrics are worse than these of the last layer. In some cases, there is no detection capability at all for the gradient scores obtained from the uniform label.

In conclusion, the gradients of the second-to-last layer do not improve the uncertainty estimation (at pixel- and segment-level) nor the OoD segmentation quality, rather they perform worse in some cases. The finding that deeper layer gradients contain less information than the final layer has been observed before outside the semantic segmentation setting by Huang et al. [2021] and Riedlinger et al. [2023].

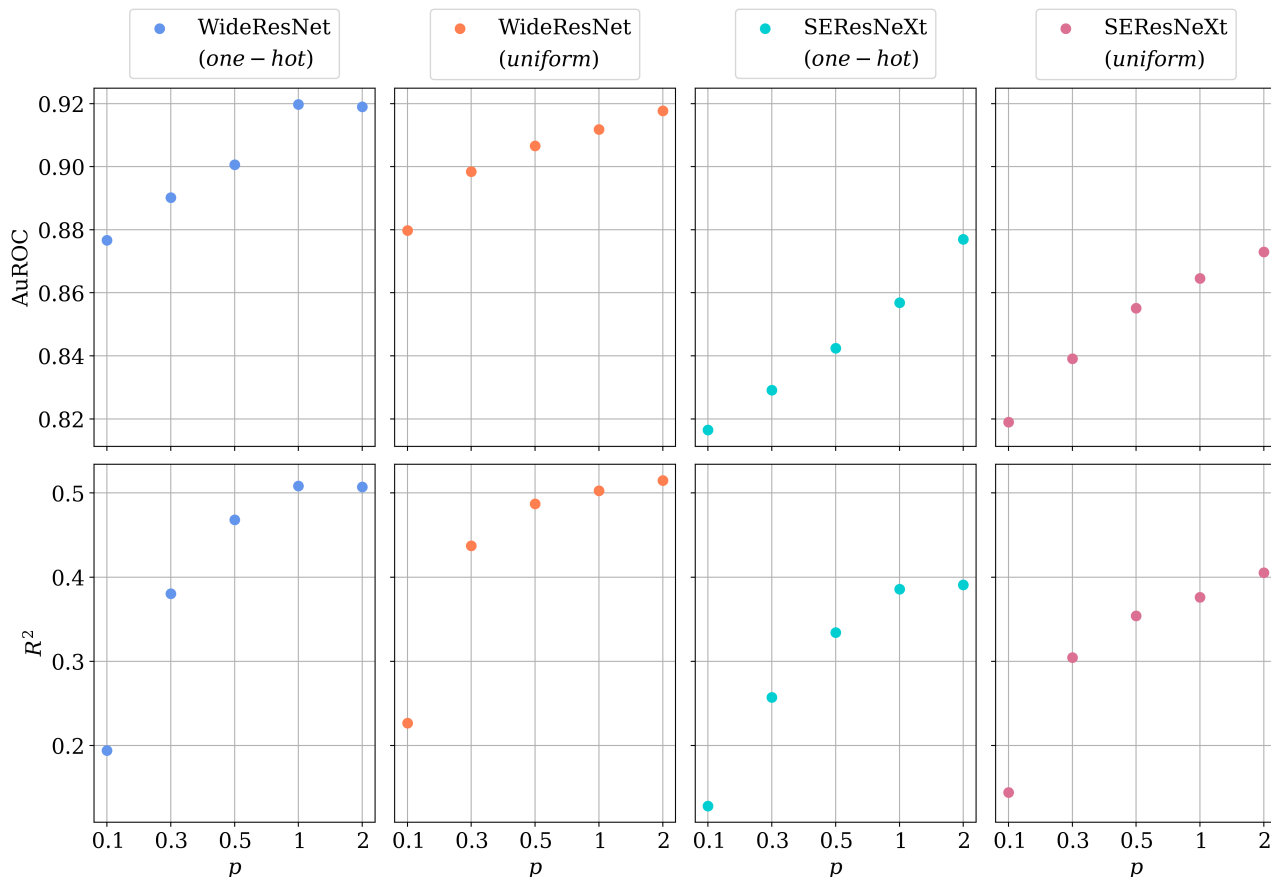


Figure 5: AuROC and R^2 values for both backbone architectures applied to the Cityscapes dataset and the different p -norms.

Table 6: Pixel-wise uncertainty evaluation results for both backbone architectures and the Cityscapes dataset as well as for different p -norms and layers in terms of ECE and AuSE.

	p	last layer		second-to-last layer	
		ECE ↓	AuSE ↓	ECE ↓	AuSE ↓
Wide-ResNet (one-hot)	0.1	0.0187	0.0500	0.0186	<u>0.0235</u>
	0.3	0.0183	0.0712	0.0125	0.0286
	0.5	0.0163	0.0508	0.0059	0.0280
	1	<u>0.0025</u>	0.0307	<u>0.0027</u>	0.0271
	2	0.0019	<u>0.0268</u>	0.0021	0.0265
Wide-ResNet (uniform)	0.1	0.0186	0.0784	0.0096	0.3347
	0.3	0.0163	0.3426	0.1846	0.6746
	0.5	0.0241	0.5857	0.3385	0.7520
	1	0.3762	0.7424	0.4345	0.8028
	2	0.3868	0.8104	0.3989	0.8253
SERes-NeXt (one-hot)	0.1	0.0347	0.0201	0.0344	0.0060
	0.3	0.0336	0.0386	0.0290	0.0353
	0.5	0.0305	0.0399	0.0214	0.0379
	1	0.0078	0.0383	0.0079	0.0377
	2	0.0039	0.0365	0.0068	0.0365
SERes-NeXt (uniform)	0.1	0.0346	0.0427	0.0295	0.1823
	0.3	0.0313	0.2484	0.1916	0.4878
	0.5	0.0076	0.5617	0.3000	0.6198
	1	0.3744	0.7694	0.4075	0.7413
	2	0.4030	0.8187	0.4003	0.8116

Table 7: Segment-wise uncertainty evaluation results for both backbone architectures and the Cityscapes dataset as well as for the different p -norms and layers in terms of classification AuROC and regression R^2 .

	p	last layer		second-to-last layer	
		AuROC ↑	R^2 ↑	AuROC ↑	R^2 ↑
Wide-ResNet (one-hot)	0.1	87.66	19.40	88.40	29.45
	0.3	89.02	38.03	90.28	48.23
	0.5	90.06	46.82	90.52	49.63
	1	91.97	<u>50.82</u>	91.04	50.28
	2	<u>91.90</u>	50.72	91.54	<u>50.54</u>
Wide-ResNet (uniform)	0.1	87.97	22.65	89.67	27.99
	0.3	89.84	43.72	90.84	45.96
	0.5	90.66	48.71	91.08	48.66
	1	91.18	50.26	<u>91.36</u>	50.48
	2	91.77	51.48	91.54	51.37
SERes-NeXt (one-hot)	0.1	81.65	12.81	81.48	2.29
	0.3	82.91	25.73	84.80	32.56
	0.5	84.24	33.43	85.28	36.21
	1	85.68	38.57	86.01	38.03
	2	87.70	39.08	87.82	39.00
SERes-NeXt (uniform)	0.1	81.90	14.41	78.49	6.06
	0.3	83.91	30.44	85.14	28.28
	0.5	85.51	35.40	85.62	33.40
	1	86.46	37.61	86.38	38.05
	2	87.30	40.54	87.31	40.38

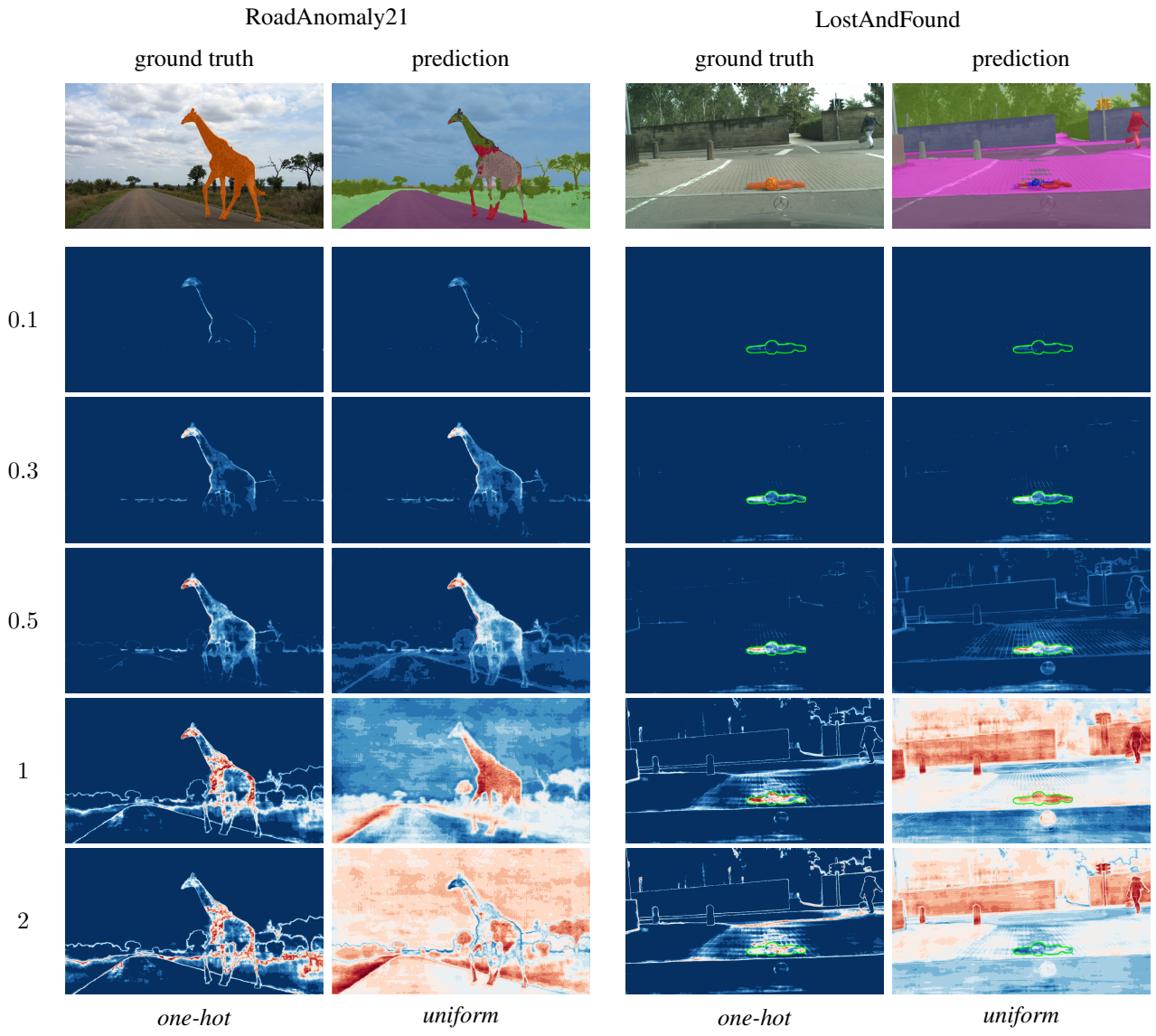


Figure 6: Ground truth (labeled OoD object), semantic segmentation prediction and PGN heatmaps for different p -norms as well as for the predictive one-hot and the uniform label, respectively.

Table 8: OoD segmentation results for the LostAndFound and the RoadObstacle21 dataset for different p -norms.

		LostAndFound					RoadObstacle21				
	p	AuPRC \uparrow	FPR ₉₅ \downarrow	sIoU \uparrow	PPV \uparrow	$\overline{F_1}$ \uparrow	AuPRC \uparrow	FPR ₉₅ \downarrow	sIoU \uparrow	PPV \uparrow	$\overline{F_1}$ \uparrow
Wide-ResNet (<i>one-hot</i>)	0.1	49.5	21.2	39.5	29.6	25.1	8.0	23.3	14.2	7.5	2.9
	0.3	64.9	15.9	48.5	<u>47.6</u>	<u>45.8</u>	16.3	<u>15.4</u>	<u>20.8</u>	14.4	<u>7.5</u>
	0.5	64.9	18.4	48.3	50.0	46.9	18.8	14.8	22.1	<u>16.5</u>	9.2
	1	44.3	25.1	25.8	40.8	21.6	<u>17.8</u>	15.5	17.1	16.9	6.1
	2	11.5	30.6	26.9	26.1	16.3	12.8	16.7	19.2	13.9	5.5
Wide-ResNet (<i>uniform</i>)	0.1	47.1	21.8	38.4	27.2	22.3	7.2	25.4	13.6	6.9	2.5
	0.3	64.8	13.5	<u>48.4</u>	44.1	43.2	14.4	17.2	18.0	13.0	6.4
	0.5	69.3	9.8	50.0	44.8	45.4	16.5	19.7	19.5	14.8	7.4
	1	57.7	10.1	33.7	35.2	27.4	8.0	62.6	5.7	8.8	1.2
	2	8.1	100.0	7.5	19.2	4.1	3.4	99.9	1.7	14.0	0.3
SERes-NeXt (<i>one-hot</i>)	0.1	66.6	5.2	43.8	35.0	34.0	3.5	39.1	5.3	6.7	1.1
	0.3	75.1	<u>4.2</u>	46.2	44.2	43.8	6.7	26.8	5.3	9.7	2.5
	0.5	70.3	7.8	43.4	44.6	41.7	8.1	24.5	5.8	10.1	3.2
	1	45.1	14.5	22.6	36.5	18.5	8.5	24.7	4.2	11.8	1.8
	2	15.1	18.7	22.8	21.9	12.8	5.6	26.2	9.0	11.3	3.1
SERes-NeXt (<i>uniform</i>)	0.1	64.7	6.1	42.8	34.9	32.4	3.2	41.3	5.7	6.1	1.0
	0.3	<u>75.0</u>	3.9	46.4	43.8	43.3	6.1	29.0	5.2	9.0	2.1
	0.5	73.8	6.9	45.1	44.8	42.3	7.4	28.7	5.7	10.3	2.7
	1	42.0	49.5	17.1	33.8	11.7	11.2	79.2	5.1	12.0	1.8
	2	5.8	100.0	3.3	15.7	1.4	9.2	99.8	1.7	15.5	1.7

Table 9: OoD segmentation results for the Fishyscapes LostAndFound and the RoadAnomaly21 dataset for different p -norms.

		Fishyscapes LostAndFound					RoadAnomaly21				
	p	AuPRC \uparrow	FPR ₉₅ \downarrow	sIoU \uparrow	PPV \uparrow	$\overline{F_1}$ \uparrow	AuPRC \uparrow	FPR ₉₅ \downarrow	sIoU \uparrow	PPV \uparrow	$\overline{F_1}$ \uparrow
Wide-ResNet (<i>one-hot</i>)	0.1	23.9	22.0	13.9	29.5	15.6	28.2	75.4	18.2	14.8	4.2
	0.3	<u>26.9</u>	31.2	16.2	30.0	<u>18.1</u>	33.8	70.5	20.9	18.4	6.0
	0.5	22.8	35.5	12.1	27.3	14.1	34.5	69.5	19.4	19.3	5.5
	1	10.1	39.1	4.0	14.6	3.3	32.5	69.5	16.1	17.0	5.8
	2	1.5	41.7	11.5	2.7	1.7	25.7	70.2	15.5	15.1	5.8
Wide-ResNet (<i>uniform</i>)	0.1	23.0	<u>21.7</u>	13.6	27.6	14.7	27.6	75.9	17.8	14.6	4.1
	0.3	28.3	29.2	<u>15.7</u>	<u>32.1</u>	18.4	33.7	69.7	20.8	17.1	5.8
	0.5	<u>26.9</u>	36.6	14.8	29.6	16.5	36.7	61.4	21.6	17.8	6.2
	1	0.8	66.4	6.2	2.5	2.0	<u>45.2</u>	<u>60.7</u>	24.8	26.2	<u>9.5</u>
	2	0.2	99.8	0.2	0.3	0.0	29.2	97.7	21.1	<u>29.0</u>	6.1
SERes-NeXt (<i>one-hot</i>)	0.1	21.0	15.6	10.4	21.2	8.3	36.2	65.7	21.9	16.9	5.7
	0.3	23.7	23.7	10.1	26.8	11.6	40.5	64.9	24.5	19.5	8.7
	0.5	20.8	29.8	8.1	23.9	9.4	39.3	66.5	23.1	21.5	7.8
	1	8.8	36.3	4.6	12.4	3.4	33.3	69.4	17.2	16.2	8.1
	2	1.2	39.4	11.5	2.2	1.6	27.1	71.0	16.2	14.0	7.4
SERes-NeXt (<i>uniform</i>)	0.1	20.6	15.6	8.1	21.6	6.6	35.6	66.2	21.3	17.0	5.3
	0.3	24.1	21.8	10.5	26.3	11.9	41.1	62.7	<u>24.9</u>	20.0	8.5
	0.5	22.6	32.0	8.6	32.3	11.0	42.8	56.4	25.8	21.8	9.7
	1	0.6	83.3	1.8	2.3	0.6	47.4	67.3	23.7	24.9	9.0
	2	0.2	99.8	0.2	0.3	0.0	35.0	98.1	22.3	30.7	8.3

Table 10: OoD segmentation results for the LostAndFound and the Fishyscapes LostAndFound dataset for different p -norms and the second-to-last layer.

		LostAndFound					Fishyscapes LostAndFound				
		AuPRC \uparrow	FPR ₉₅ \downarrow	sIoU \uparrow	PPV \uparrow	$\overline{F_1}$ \uparrow	AuPRC \uparrow	FPR ₉₅ \downarrow	sIoU \uparrow	PPV \uparrow	$\overline{F_1}$ \uparrow
Wide-ResNet (<i>one-hot</i>)	0.1	10.3	40.0	12.6	15.8	4.0	2.0	<u>36.8</u>	1.6	3.0	0.6
	0.3	10.9	32.9	23.1	23.0	11.3	1.7	39.4	2.3	2.2	0.5
	0.5	<u>10.5</u>	32.4	26.9	25.5	15.3	1.5	40.3	9.6	2.3	1.3
	1	10.0	32.2	<u>28.9</u>	26.1	<u>17.3</u>	1.4	41.1	<u>12.2</u>	2.5	<u>1.9</u>
	2	9.7	32.1	30.0	<u>25.7</u>	18.3	1.3	41.5	13.6	2.8	2.4
Wide-ResNet (<i>uniform</i>)	0.1	0.7	98.8	0.5	0.8	0.0	0.3	96.0	0.8	0.7	0.0
	0.3	0.5	99.8	0.5	0.8	0.0	0.2	98.9	0.2	0.3	0.0
	0.5	0.5	99.9	0.5	0.8	0.0	0.2	99.5	0.2	0.3	0.0
	1	0.5	100.0	0.5	0.8	0.0	0.2	99.7	0.2	0.3	0.0
	2	0.5	100.0	0.5	0.8	0.0	0.2	99.8	0.2	0.3	0.0
SERes-NeXt (<i>one-hot</i>)	0.1	3.0	66.2	4.9	7.3	1.4	<u>1.9</u>	41.1	5.8	5.2	1.8
	0.3	6.8	27.1	15.4	12.9	6.1	<u>1.9</u>	36.0	5.2	<u>5.0</u>	1.6
	0.5	8.1	23.9	19.5	15.2	8.6	1.7	<u>36.8</u>	4.1	4.3	1.0
	1	9.3	<u>21.7</u>	22.6	17.8	11.1	1.4	37.6	7.0	2.1	0.9
	2	10.4	20.4	24.1	18.4	12.7	1.2	38.3	11.5	2.3	1.7
SERes-NeXt (<i>uniform</i>)	0.1	0.4	99.9	0.5	0.8	0.0	0.2	88.9	0.3	0.0	0.0
	0.3	0.4	99.9	0.5	0.8	0.0	0.2	93.2	0.2	0.0	0.0
	0.5	0.4	100.0	0.5	0.8	0.0	0.2	96.1	0.2	0.3	0.0
	1	0.4	100.0	0.5	0.8	0.0	0.2	99.2	0.2	0.3	0.0
	2	0.5	100.0	0.5	0.8	0.0	0.2	99.7	0.2	0.3	0.0